STATE OF THE CLIMATE IN 2018

Special Supplement to the
Bulletin of the American Meteorological Society
Vol. 100, No. 9, September 2019

era (circa 2005), does not. It is likely the different methods for dealing with under-sampled regions in analyses cause the disagreement in the long-term trends for the 700–2000-m layer OHCA estimates. For 2000–6000 m, the linear trend is 0.07 (±0.04) W m^{-2} from September 1992 to May 2011, using repeat hydrographic section data collected from 1981 to 2018 to update the estimate of Purkey and Johnson (2010). Summing the three layers (with their slightly different time periods), the full-depth ocean heat gain rate ranges from 0.57 to 0.81 W m^{-2} roughly applicable to 1993–2018. Estimates starting circa 2005 have much smaller uncertainties, e.g., 0.61 ± 0.09 W m^{-2} for ocean warming at depths of 0–1800 dbar during 2005–15 (Johnson et al. 2016).

Table 3.2. Trends of ocean heat content increase (in W m^{-2} applied over the 5.1 × 10^{14} m^2 surface area of Earth) from seven different research groups over three depth ranges (see Fig. 3.6 for details). For the 0–700- and 700–2000-m depth ranges, estimates cover 1993–2018, with 5%–95% uncertainties based on the residuals taking their temporal correlation into account when estimating degrees of freedom (Von Storch and Zwiers 1999). The 2000–6000-m depth range estimate, an update of Purkey and Johnson (2010), uses data from 1981 to 2018, but the globally averaged first and last years are 1992.7 and 2011.4, again with 5%–95% uncertainty.

Research group	Global ocean heat content trends (W m^{-2}) for three depth ranges		
	0–700 m	700–2000 m	2000–6000 m
MRI/JMA	0.36 ± 0.06	0.24 ± 0.05	—
CSIRO/ACE/CRC/IMAS/UTAS	0.42 ± 0.06	—	—
PMEL/JPL/JIMAR	0.39 ± 0.14	0.32 ± 0.03	—
NCEI	0.38 ± 0.06	0.19 ± 0.06	—
Met Office Hadley Centre	0.36± 0.15	0.14 ± 0.05	—
IAP/CAS	0.39 ± 0.05	0.18 ± 0.02	—
Purkey and Johnson update	—	—	0.07 ± 0.04

d. Salinity—G. C. Johnson, J. Reagan, J. M. Lyman, T. Boyer, C. Schmid, and R. Locarnini

1) Introduction—G. C. Johnson and J. Reagan

Salinity is the fraction of dissolved salts in water, nominally in g kg^{-1}, but measured and reported here as a dimensionless quantity on the 1978 Practical Salinity Scale, or PSS-78 (Fofonoff and Lewis 1979). Salinity and temperature together determine the density of seawater at a given pressure. Their variability can alter the density patterns that are integral to the global thermohaline circulation (e.g., Gordon 1986; Broecker 1991). One prominent limb of the global thermohaline circulation, the AMOC, is particularly susceptible to changes in salinity (e.g., Liu et al. 2017). Salinity is also a conservative water property, traceable back to where a water mass was originally formed at the surface and subducted into the ocean's interior (e.g., Skliris et al. 2014). Where precipitation dominates evaporation, fresher surface seawater is found (i.e., along the ITCZ and at high latitudes), and where evaporation dominates precipitation, saltier surface seawater is found (i.e., in the subtropics). Salinity acts as a natural rain gauge (e.g., Terray et al. 2012), useful since ~80% of the global hydrological cycle takes place over the ocean (e.g., Durack 2015). Salinity changes are used to estimate changes in the hydrological cycle (e.g., Durack et al. 2012). They also play a role in local sea level changes through seawater contraction with salinification and expansion with freshening (e.g., Durack et al. 2014). Finally, besides atmospheric freshwater fluxes, other factors can modify salinity such as advection, mixing, entrainment, sea ice melt/freeze, and river runoff (e.g., Ren et al. 2011).

Different data sources are used for different salinity analyses in this section owing to data availability and accuracy. To investigate interannual changes of subsurface salinity, all available salinity profile data are quality controlled following Boyer et al. (2013) and then used to derive 1° monthly mean gridded salinity anomalies relative to a long-term monthly mean for years 1955–2012 [World Ocean Atlas 2013 version 2 (WOA13v2); Zweng et al. 2013] at standard depths from the surface to 2000 m (Boyer et al. 2013). In recent years, the largest source of salinity profiles is the Argo program (Riser et al. 2016). These data are a mix of real-time (preliminary) and delayed-mode (scientific quality controlled) observations. Hence, the estimates presented here could change after all data are subjected to scientific quality control. The sea surface salinity (SSS) analysis relies on Argo data downloaded in January 2019, with annual maps generated following Johnson and Lyman (2012) as well as monthly maps of bulk (as opposed to skin) SSS data from the Blended Analysis of Surface Salinity (BASS) (Xie et al. 2014). BASS blends in situ SSS data with data from the Aquarius (Le Vine et al. 2014; mission ended in June 2015), Soil Moisture and Ocean Salinity (SMOS; Font et al. 2013), and recently Soil Moisture Active Passive (SMAP; Fore et al. 2016) satellite

missions. BASS maps can be biased fresh around land (including islands), and features at high latitudes should be validated with in situ maps. Despite the larger uncertainties of satellite data relative to Argo data, their higher spatial and temporal sampling allows higher spatial and temporal resolution maps than are possible using in situ data alone at present.

2) Sea surface salinity—G. C. Johnson and J. M. Lyman

Extratropical 2018 SSS anomalies (Fig. 3.7a, colors) exhibit large-scale similarities with those from 2004 to 2017 (see previous *State of the Climate* reports). With the partial exception of the North Pacific in 2018 and 2017, subtropical salinity maxima are mostly salty with respect to the WOA13v2 climatology. The fresher higher latitude regions such as the subpolar North Pacific, the Irminger and portions of the Nordic seas of the North Atlantic, and some portions of the Southern Ocean are anomalously fresh with respect to climatology. A warmer atmosphere can hold more water, withdrawing more in evaporative regions and depositing more in precipitation-prone regions, which would lead to the salinity patterns observed (Rhein et al. 2013), as well as those seen in the extratropical 2005–18 trends discussed below. Within the tropics, which have large SSS excursions with ENSO and other interannual variations, both the ITCZ and SPCZ in the Pacific are quite fresh in 2018 with respect to climatology (Fig. 3.7a), as is the region near the Amazon and Orinoco river mouths in the Atlantic.

A tight relationship between anomalies of air–sea freshwater fluxes (precipitation minus evaporation; $P - E$) and SSS anomalies is especially apparent in the year-to-year changes of both quantities. Where SSS changes from 2017 to 2018 (Fig. 3.7b, colors) are positive, $P - E$ tendencies over that same period are often negative (see Fig. 3.12b). With a reduction in rainfall from 2017 to 2018 around the Maritime Continent, that region between the Indian and Pacific Oceans sees an increase in SSS from 2017 to 2018. With increased freshwater flux into the ocean around the Pacific ITCZ, the SSS in the region decreases from 2017 to 2018, whereas south of the equator the opposite pattern holds. This relationship can also be seen in the freshening tropical Indian Ocean, the salinifying subtropical North Pacific, and the freshening Gulf of Alaska, among other regions. The freshening SSS tendency from 2017 to 2018 just south of the equator in the Indian Ocean may be partly owing to an increase in anomalous westward currents between 2017 and 2018 there (see Fig. 3.18b) in the presence of mean SSS that increases from east to west.

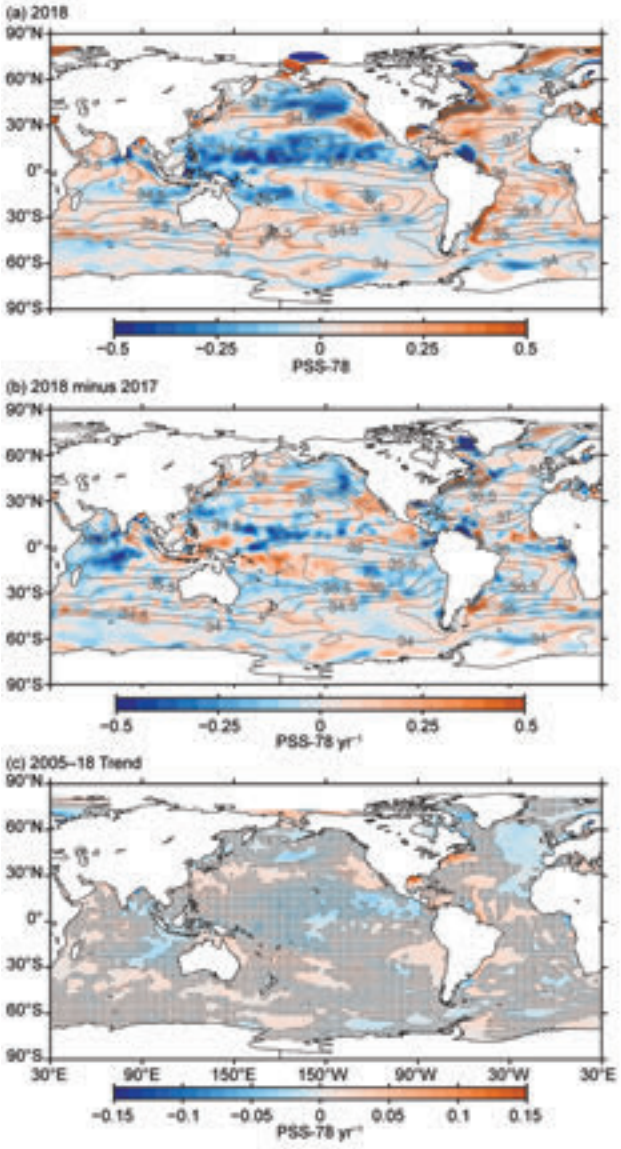

Fig. 3.7. (a) Map of the 2018 annual surface salinity anomaly (colors, PSS-78) with respect to monthly climatological 1955–2012 salinity fields from WOA13v2 (long-term average—gray contours at 0.5 intervals, PSS-78). (b) Difference of 2018 and 2017 surface salinity maps (colors, PSS-78 yr^{-1}). White ocean areas are too data-poor (retaining < 80% of a large-scale signal) to map. (c) Map of local linear trends estimated from annual surface salinity anomalies for 2005–18 (colors, PSS-78 yr^{-1}). Areas with statistically insignificant trends at 5%–95% confidence are stippled. All maps are made using Argo data downloaded in Jan 2019.

As in 2017, strong seasonal variations of BASS (Xie et al. 2014) SSS anomalies (Fig. 3.8) are evident near the Amazon and Orinoco River plumes in 2018. For the first three quarters of the year, there is a fresh anomaly localized near the coast, but it extends eastward across much of the northern equatorial Atlantic in September–November. In the tropical Pacific, a

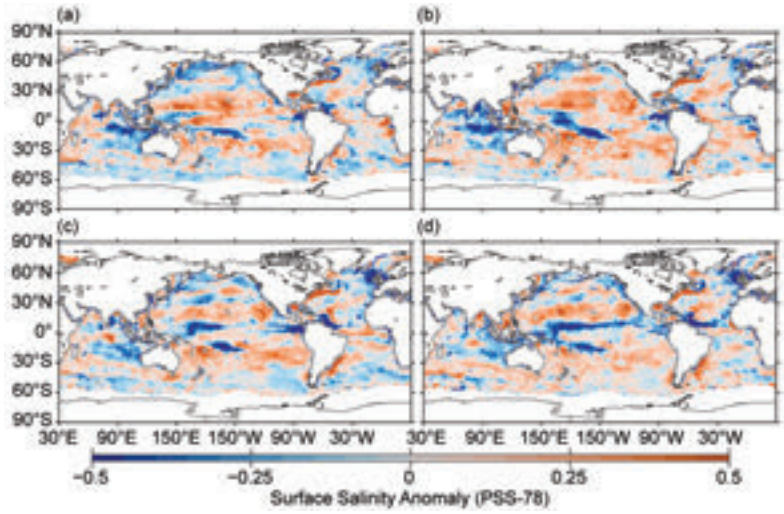

Fig. 3.8. Seasonal maps of SSS anomalies (colors) from monthly blended maps of satellite and in situ salinity data (BASS; Xie et al. 2014) relative to monthly climatological 1955–2012 salinity fields from WOA13v2 for (a) Dec 2017–Feb 2018, (b) Mar–May 2018, (c) Jun–Aug 2018, and (d) Sep–Nov 2018. Areas with maximum monthly errors exceeding 10 PSS-78 are left white.

fresh anomaly builds under the ITCZ in June–August and strengthens in September–November.

Sea surface salinity trends for 2005–18, the era of near-global Argo coverage, are estimated by local linear fits to annual average SSS maps from Argo data (Fig. 3.7c). Large-scale patterns of local trends have not changed much from last year's report. Regions with already high salinity values, such as the subtropical salinity maxima in all the ocean basins and the Arabian Sea, show increasing trends, with statistical significance in some portions of those regions, especially in the South Indian Ocean and in the Pacific off the west coasts of the Americas. Statistically significant freshening trends are apparent in the subpolar North Pacific, the eastern subpolar North Atlantic, the eastern warm fresh pool in the tropical North Pacific, and the Bay of Bengal. These are all regions that are climatologically fresh relative to their surroundings. In the Gulf of Mexico and along the east coast of North America from roughly Cape Hatteras northward, strong, statistically significant trends toward saltier and warmer (Section 3c) conditions are evident.

3) Subsurface salinity—J. Reagan, T. Boyer, C. Schmid, and R. Locarnini

The 2009–18 basin-average monthly salinity anomalies (Fig. 3.9a) for the Atlantic Ocean continued the same pattern that has been evident for the past decade, with weak anomalies (< |0.005|) below ~600 m and salty anomalies (> 0.005) extending and increasing from ~600 m to the surface where they reach values exceeding 0.05. There is freshening (~−0.015) between 2017 and 2018 in the upper 50 m with salinification extending from 100 m to 1200 m and a maximum (~0.01) around 150 m (Fig. 3.9b). The deeper (250–700 m) salinification tendency in 2018 may be related to the deepening of the salinity anomalies from 2017 (Fig. 3.9a). 2018 is also the first year in the past decade when all 0–1500-m basin-average monthly salinity anomalies were saltier than the long-term mean (Fig. 3.9a).

The 2018 Pacific Ocean basin-average monthly salinity anomalies for 0–1500 m continued the same pattern that has been evident since mid-2014 (Fig. 3.9c). There are fresh anomalies in the upper 100 m, salty anomalies from 100–250 m, fresh anomalies from 275–600 m, and weak (< |0.005|) anomalies at depths below 600 m (Fig. 3.9c). Changes from 2017 to 2018 (Fig. 3.9d) include freshening in the upper ~100 m (max of ~−0.015 at 50 m) and salinification from 125–375 m (max of ~0.015 at 200 m). These tendencies are very similar to what was seen between 2016 and 2017 (see Fig. 3.9d in Reagan et al. 2018). 2018 also marks the fourth straight year with fresh anomalies in the upper 100 m, following a 5-year period (2009–14) of persistent salty anomalies in the upper 100 m (Fig. 3.9c). A possible cause for these persistent anomalies may be related to in-phase transitions of ENSO and PDO (see discussion in Reagan et al. 2018).

The Indian Ocean basin-average monthly salinity anomalies experienced persistent fresh anomalies in the upper 0–100/200 m from mid-2011 through mid-2016, with salty anomalies in a 100–200-m thick layer below (Fig. 3.9e). The 0–100-m salinity exceeded the long-term average in mid-2016 through early 2018, followed by some near-surface (< 50 m) freshening evident in mid-2018. There are also salty anomalies extending from the surface to depths of ~700 m during the latter half of 2018 (Fig. 3.9e). The major change between 2017 and 2018 was very strong freshening (< ~−0.025) in the upper 30 m (Fig. 3.9f), discussed further below.

The zonally-averaged salinity tendency from 2017 to 2018 in the upper 500 m of the Atlantic Ocean shows strong freshening in the upper 50 m along the equator (max < −0.15 at 0 m, Fig. 3.10a) which is associated with a narrow strip of near-surface fresh-

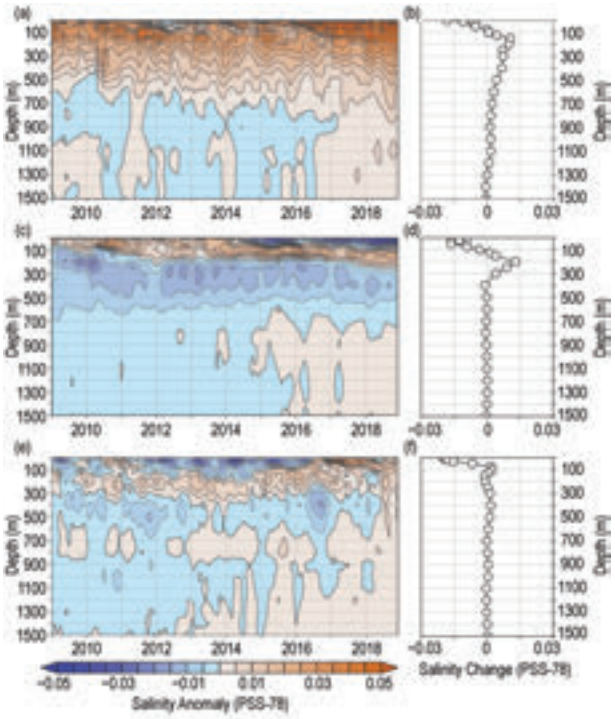

Fig. 3.9. Average monthly salinity anomalies from 0–1500 m for the (a) Atlantic from 2009–18 and (b) the change from 2017 to 2018; (c) Pacific from 2009–18 and (d) the change from 2017 to 2018; (e) Indian from 2009–18 and (f) the change from 2017 to 2018. Data were smoothed using a 3-month running mean. Anomalies are relative to the long-term WOA13v2 monthly salinity climatology for years 1955–2012 (Zweng et al. 2013).

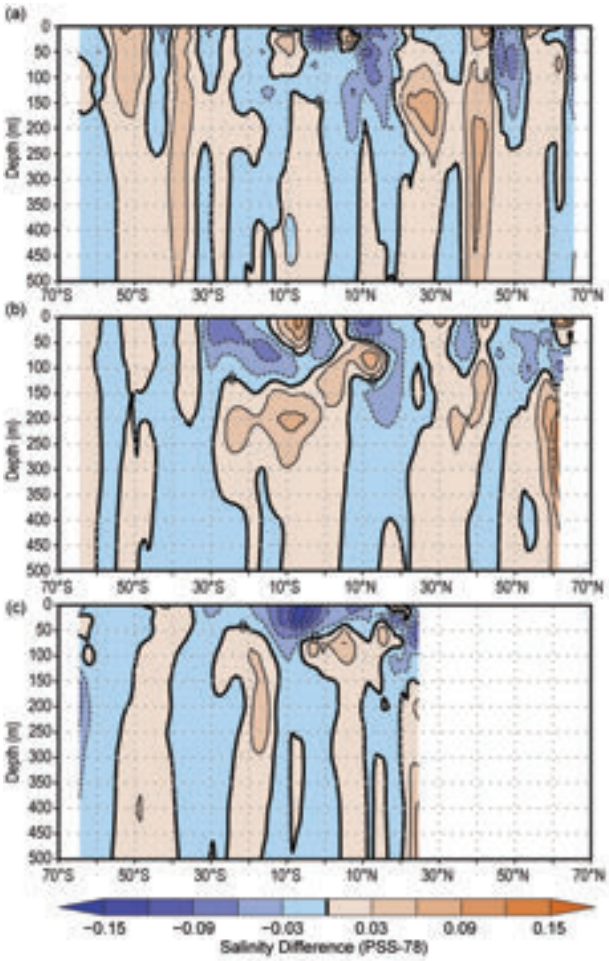

Fig. 3.10. Difference between the 2018 and 2017 zonal average monthly salinity anomalies from 0–500m for the (a) Atlantic, (b) Pacific, and (c) Indian Ocean basins. Anomalies are relative to the long-term WOA13v2 monthly salinity climatology for years 1955–2012 (Zweng et al. 2013). Contours represent multiples of ±0.03 with a bold 0 contour.

ening between the Gulf of Guinea and Northeast Brazil (Fig. 3.7b). Additionally, there is freshening (< −0.03) from 10° to 20°N extending from 0 m to 200 m. There is also freshening from 45° to 52°N in the upper 150 m, which is opposite to the salinification observed between 2016 and 2017 (see Fig. 3.10a in Reagan et al. 2018). Finally, there is salinification (> 0.03) from 0 m to 500 m near 40°N and 40°S, from 0 m to 175 m between 48°–55°S, and a subsurface area from 20°–30°N at 75–250 m (Fig. 3.10a).

The changes in the Pacific Ocean zonally-averaged salinity from 2017 to 2018 are mainly confined to the upper 300 m (Fig. 3.10b). There is freshening (< −0.03) from 18°–32°S and 0–75 m that deepens northward to 10°S and 100 m, freshening from 8° to 16°N and 0–40 m, and salinification from 4°–12°S and 0–50 m. The latter freshening and salinification tendencies are likely associated with changes in oceanic freshwater gains and losses from evaporation and precipitation (see Fig. 3.12b). All of the aforementioned freshening and salinification tendencies shifted southward from where they were located the previous year (see Fig. 3.10b in Reagan et al. 2018). Finally, there was also salinification (> 0.03) in two subsurface Pacific regions, one centered at 10°S and 200 m and the other at greater depths between 125–500 m northward of 55°N.

Much of the larger changes (> |0.03|) of the zonally averaged salinity anomalies from 2017 to 2018 in the Indian Ocean occurred in the upper 100 m (Fig. 3.10c). There was freshening from 20°S to 10°N in the 0–50 m layer, which is a complete reversal of the prominent salinification observed there between 2016 and 2017 (see Fig. 3.10c in Reagan et al. 2018). This freshening may be due to anomalous westward surface currents (see Fig. 3.18b) in the equatorial Indian Ocean transporting fresher water westward, a reversal from what was observed last year (Johnson and Lyman 2018). Much of this freshening is located in the Arabian Sea and the central and western

portions of the tropical Indian Ocean, northward of 15°S (Fig. 3.8b). There is also freshening in the upper 150 m northward of 20°N from 2017 to 2018.

e. *Global ocean heat, freshwater, and momentum fluxes*—L. Yu, X. Jin, P. W. Stackhouse, A. C. Wilber, S. Kato, N. G. Loeb, and R. A. Weller

The ocean and the atmosphere communicate via interfacial exchanges of heat, freshwater, and momentum. These air–sea fluxes are the primary mechanisms for keeping the global climate system in near balance with the incoming insolation at Earth's surface. Most of the shortwave radiation (SW) absorbed by the ocean's surface is vented into the atmosphere by three processes: longwave radiation (LW), turbulent heat loss by evaporation (latent heat flux, or LH), and by conduction (sensible heat flux, or SH). The residual heat is stored in the ocean and transported away by the ocean's surface circulation, forced primarily by the momentum transferred to the ocean by wind stress. Evaporation connects heat and moisture transfers, and the latter, together with precipitation, determines the local surface freshwater flux. Identifying changes in the air–sea fluxes is essential in deciphering observed changes in ocean circulation and its transport of heat and salt from the tropics to the poles.

Air–sea heat flux, freshwater flux, and wind stress in 2018 and their relationships with ocean surface variables are examined here. The net surface heat flux, Q_{net}, is the sum of four terms: SW + LW + LH + SH. The net surface freshwater flux into the ocean (neglecting riverine and glacial fluxes from land) is simply Precipitation (P) minus Evaporation (E), or the $P - E$ flux. Wind stress is computed from satellite wind retrievals using the bulk parameterization of Edson et al. (2013). The production of the global maps of Q_{net}, $P - E$, and wind stress (Figs. 3.11–3.13) and the long-term perspective of the change of the forcing functions (Fig. 3.14) is made possible through integrating multi-group efforts. Ocean-surface LH, SH, E, and wind stress are from the OAFlux project's newly developed satellite-derived, high-resolution (hereafter OAFlux-HR) products (Yu and Jin 2014; Yu 2019). Surface SW and LW radiative fluxes are from the CERES Fast Longwave And Shortwave Radiative Fluxes (FLASHFlux) Ed3A product (Stackhouse et al. 2006). Global P is from the GPCP version 2.3 products (Adler et al. 2003). The CERES Energy Balanced and Filled (EBAF) surface SW and LW version 4.0 products (Loeb et al. 2018; Kato et al. 2018) are used in the time series analysis.

1) Surface heat fluxes

The dominant features in the 2018 Q_{net} anomaly field (Fig. 3.11a) are the broad-scale oceanic heat gain (positive Q_{net} anomalies) in the equatorial and southern Pacific and Indian Oceans (40°S–10°N), and the oceanic heat loss (negative Q_{net} anomalies) in the subtropical North Pacific (10°–30°N), the North Atlantic (10°–60°N), and the southern higher latitudes (40°S poleward). Positive and negative anomalies both exceeded 25 W m^{-2}. The 2018-minus-2017 Q_{net} tendency field (Fig. 3.11b) was predominantly determined by the LH + SH change pattern. The spatial pattern of Q_{net} tendencies is similar to that of the 2018-minus-2017 anomaly pattern (Fig. 3.11b) over most of the global ocean, showing that the 2018 anomalies were a strong departure from the climatological mean state. However, the two patterns differ considerably in a few regions, most notably the tropical Pacific where the 2018 tendencies have signs opposite to the

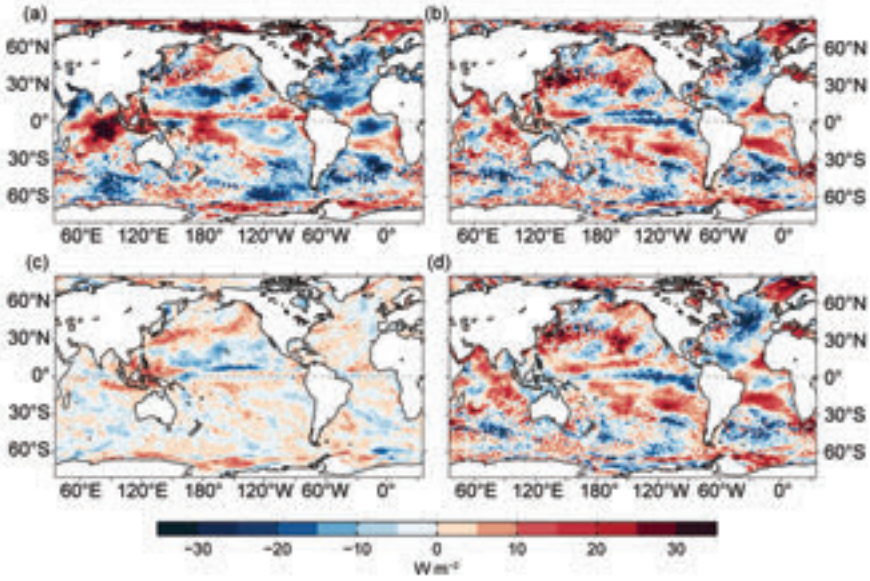

Fig. 3.11. (a) Surface heat flux (Q_{net}) anomalies (W m^{-2}) for 2018 relative to a 5-yr (2010–14) mean. Positive values denote ocean heat gain. (b) 2018 minus 2017 tendency for Q_{net}, (c) surface radiation (SW+LW), and (d) turbulent heat fluxes (LH+SH), respectively. Positive tendencies denote more ocean heat gain in 2018 than in 2017, consistent with the reversal of the color scheme in (d). LH+SH are produced by the OAFlux high-resolution (HR) satellite-based analysis, and SW+LW by the NASA FLASHFlux project.